THE JOURNAL OF PHYSICAL CHEMISTRY C
A JOURNAL OF THE AMERICAN CHEMICAL SOCIETY

pubs.acs.org/JPCC
Article

Modification of the Photochromic Properties of Oxygen-Containing Yttrium Hydride by Irradiation with keV and MeV Ions

D. Moldarev,* M. Wolff, and D. Primetzhofer

Cite This: J. Phys. Chem. C 2023, 127, 24676−24682
Read Online

ACCESS | Metrics & More | Article Recommendations

ABSTRACT: The effect of irradiation using energetic ions on the optical properties of photochromic YHO was studied. Films were exposed to different fluences (Φ); projectiles and their primary energies were chosen such that a wide range of ratios between energies transferred to electron and nuclear systems is covered. Structural modifications are found to induce a decrease in transmittance, magnitude of the photochromic response, and the bleaching kinetics. For irradiation with 330 keV Ne^+, X-ray diffraction revealed changes in the microstructure such as grain growth for higher fluences explaining the observed persistency of changes in optical properties after irradiation. On the other hand, the degradation of photochromic properties was found to be reversible for $\Phi = 1 \times 10^{15}$ cm^{-2}. The results indicate that grain boundary diffusion is necessary for the photochromic reaction.

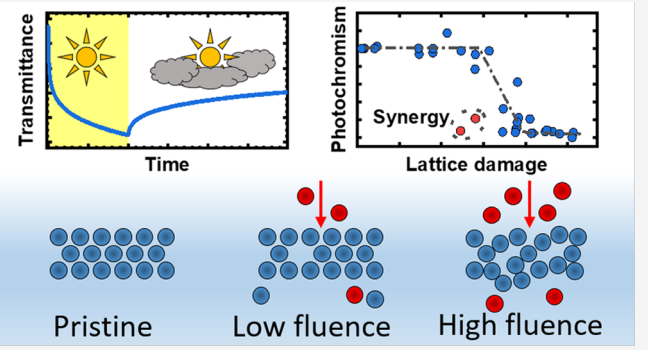

1. INTRODUCTION

Photochromic materials feature a change in optical properties as a response to electromagnetic irradiation, which makes them enticing for a vast number of applications in different fields like smart windows, sensors, and ophthalmology.[1,2] Oxygen-containing yttrium hydride (YHO)[3] along with some other oxygen-containing rare-earth metal hydrides (ScHO, NdHO, GdHO, DyHO, and ErHO)[4,5] were shown to feature a color-neutral photochromic effect at ambient conditions. The effect persists when the films are coated with a protective layer (Al_2O_3 or Si_3N_4)[6] enabling their utilization in multilayered structures.[7] Thin films of YHO are typically produced by either reactive magnetron sputtering[3] or e^- beam evaporation[8] of yttrium dihydride followed by oxidation and they show photochromic properties in a range of chemical compositions with the oxygen to yttrium ratio δ of $0.5 < \delta < 1.5$.[9] Moreover, photochromism is commonly coupled to photoconductivity,[3,10] even though the latter one is also found in YHO films with $\delta < 0.5$.[11]

While the dependency of the photochromic behavior of YHO on chemical composition, thickness, and environment have been studied extensively,[9,12] the fundamental mechanism underlying the photochromic effect remains debated. For GdHO thin films, Hans et al. showed a dual-phase nature of the material and proposed a photoinduced transfer of hydrogen between the two phases linked to the residual stress of several GPa as a mechanism of the photochromic behavior.[13] Earlier, an analogous model was suggested for YH_x photochromic foils under applied high pressure.[14] Studies employing positron annihilation spectroscopy revealed the irreversible formation of divacancies under illumination, supporting conjectures about mobile species in the material.[15] The authors hypothesized that metallic domains, formed under illumination, give rise to an increased absorption of light and put forward two possible mechanisms of domain formation: by the light-induced transport of H together with local O displacement or by the trapping of photoexcited electrons by hydrogen vacancies, created under illumination. An enhanced bleaching rate was achieved using aliovalent Ca doping, which decreased the H content in the film.[16] The result was attributed to the increased number of anion vacancies, simplifying H migration through interstitial sites. The importance of defects for photochromic properties was pointed out in ref 17 as well, where the annealing of photochromic YHO films at 87 °C resulted in slower bleaching.

Despite the diversity of the detailed mechanisms proposed to explain the photochromic effect, their common basis is a photoinduced migration of anions, primarily H^-, where anion vacancies and other defects serve as a pathway for this migration. Defect engineering offers a potential method of

Received: September 6, 2023
Revised: November 27, 2023
Accepted: November 28, 2023
Published: December 14, 2023

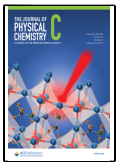

https://doi.org/10.1021/acs.jpcc.3c06010
J. Phys. Chem. C 2023, 127, 24676−24682

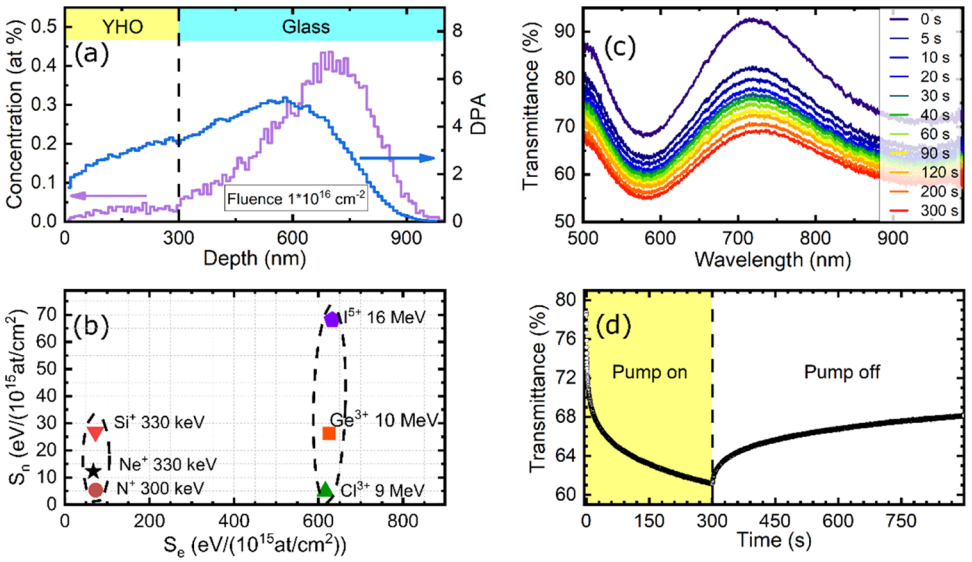

Figure 1. (a) Implantation (left axis) and damage profile (right axis) for YHO on glass under 330 keV Ne^+ irradiation to an ion fluence of 1×10^{16} cm^{-2}, as calculated by SRIM. (b) Nuclear and electronic stopping cross-sections of YHO for 300 keV N^+, 330 keV Ne^+, 330 keV Si^+, 9 MeV Cl^{3+}, 10 MeV Ge^{3+}, and 16 MeV I^{5+}, as predicted by SRIM. Dashed lines highlight the irradiation series with "low" and "high" S_e. (c) Evolution of the spectral transmittance of the photochromic YHO film for different illumination times. (d) Average transmittance of the YHO film under illumination and during bleaching.

tailoring the photochromic performance of REHO. Ion irradiation is a powerful tool for achieving controlled structural modification and is widely used for materials engineering.[18] Energetic ions traversing a material transfer energy to its nuclear and electron systems, leading to the formation of crystal defects[19] or their annealing, depending on which process prevails at the given irradiation conditions.[20] For example, ion irradiation was employed for graphene nanopatterning[21] and to improve the hydrogen evolution reaction performance of MoS_2.[22]

In this work, we irradiate ~300 nm thick photochromic YHO thin films with keV and MeV ions. In order to distinguish between the effects of ion interaction with nuclei, resulting in displacements, and with electrons, resulting in ionization and a thermal spike along the trajectory, projectiles and their primary energies were selected to feature different ratios of the nuclear stopping power cross-section (S_n) to the electronic stopping power cross-section (S_e). We find a decrease in optical transmittance, photochromic response, and bleaching speed after irradiation. The reversibility of those changes for lower fluences is demonstrated. The implication of the obtained results for the mechanism of photochromic behavior is discussed in the context of the dual-phase nature of YHO.

2. EXPERIMENTAL DETAILS

Photochromic films were prepared by reactive magnetron sputtering using a Y target (99.9% nominal bulk purity) as the cathode. First, a 300 nm YH_2 precursor was deposited in a mixed Ar and H_2 atmosphere on soda-lime glass (a 1 mm thick microscope slide) precleaned using isopropanol and deionized water. The base pressure in the chamber before deposition was below 5×10^{-5} mbar. The total deposition pressure was kept in the range of $(0.6-1) \times 10^{-2}$ mbar. No deliberate heating of the substrate was used during the deposition process. As a second step, films were oxidized by venting the chamber, and YHO was formed. To hinder further compositional modification, the films were stored in a vacuum desiccator until their characterization and ion irradiation. For more details on the preparation of photochromic films, we refer to ref 5[5].

Ion irradiation was conducted at the 350 kV Danfysik implanter and the 5 MV NEC Pelletron accelerator, both located at the Tandem Laboratory of Uppsala University.[23] To elucidate the potential specific effects of ion irradiation on the nuclear and electronic subsystems of YHO, two series of irradiation conditions (projectiles and their primary energies) having a comparably "low" S_e (≈70 eV/(10^{15} at/cm^2)) and a "high" S_e (≈620 eV/(10^{15} at/cm^2)) with different S_n were selected. In addition, the average projected range of ions in the sample was chosen to be larger than the thickness of the film to avoid a significant implantation into YHO. This procedure also ensures that different depths of the film are affected in a similar way by the irradiating species. Irradiation was carried out using beams of 300 keV N^+, 330 keV Ne^+, and 330 keV Si^+ (all three with "low" S_e) and 9 MeV Cl^{3+}, 10 MeV Ge^{3+}, and 16 MeV I^{5+} (all three with "high" S_e). Both S_e and S_n predicted by Monte Carlo simulations using SRIM-2013[24] assuming an equiatomic YHO compound with a bulk density of 6.44×10^{22} at/cm^3[12] are summarized in Figure 1b. To assess the induced lattice damage, i.e., displacements per atom (dpa) associated with the ion bombardment, full damage cascade simulations employing SRIM-2013 were performed with the displacement energy, as well as bulk and surface binding energies, for different atoms listed in Table 1. The results of the simulation, the profile of the implanted ions on the left axis, and the introduced damage on the right axis for 330 keV Ne^+ irradiation to an ion fluence

Table 1. Input Parameters Such as Displacement Energy, Lattice Binding Energy, and Surface Binding Energy Used for SRIM Simulations

atoms	displacement E, eV	lattice binding E, eV	surface binding E, eV
Y	25	3	4.24
H	10	3	2
O	28	3	2

https://doi.org/10.1021/acs.jpcc.3c06010
J. Phys. Chem. C 2023, 127, 24676−24682

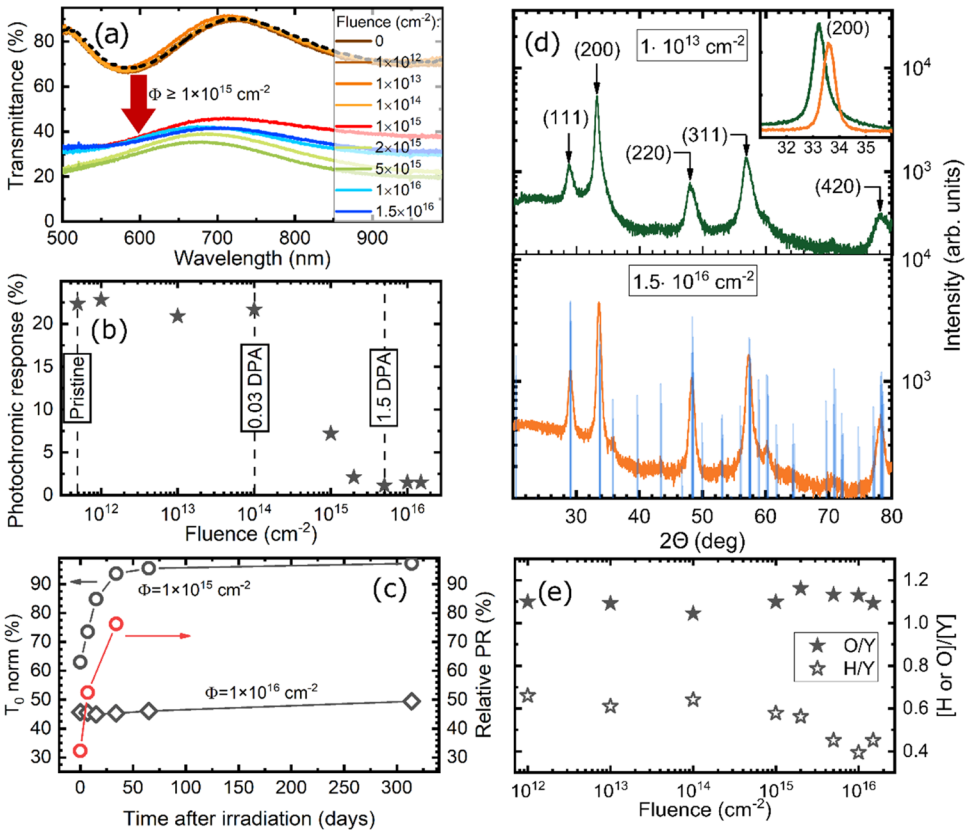

Figure 2. Effect of 330 keV Ne^+ irradiation with different total fluences on the (a) optical transmittance and (b) photochromic response of YHO films. The dashed line in panel (a) is the result for the irradiation from the back side to a fluence of 1×10^{15} cm^{-2}. (c) Normalized average transmittance and photochromic response measured at different times after ion irradiation. (d) GIXRD patterns measured for films irradiated with 330 keV Ne^+ to an ion fluence of 1×10^{13} and 1.5×10^{16} cm^{-2}. The inset shows a close-up of the (200) peak for both fluences. Blue vertical lines represent the ICDD powder diffraction file 04−026−1364. (e) Oxygen or hydrogen to yttrium ratio deduced from ToF-E ERDA.

of 1×10^{16} cm^{-2} are shown in Figure 1a. While the peak concentration of the implanted species (~0.4 at. %) is located hundreds of nanometers deep in the substrate, the irradiation leads to an average Ne concentration in the YHO film of 0.03% and an average damage of 2.8 dpa.

The optical transmittance of YHO films was measured by using a stabilized tungsten-halogen light source in conjunction with a compact CCD spectrometer (ThorLabs CCS200). A photochromic transition was triggered by illuminating the films with a 405 nm LED (a nominal irradiance of 14.53 $\mu W/mm^2$). More details on the optical setup can be found elsewhere.[25] Typical transmittance spectra of a YHO film before illumination and after different illumination times are presented in Figure 1c. Samples were illuminated for 300 s followed by 600 s of bleaching. Figure 1d shows the time evolution of transmittance averaged in the wavelength range of 500−900 nm and plotted over time. Quantification of the photochromic response was done by calculating the relative change in average transmittance after 300 s of illumination $(T_{300}-T_0)/T_0$. The bleaching time constant τ was determined from the linear slope of the equation $\ln(-\ln(T/T_0)) = -1/\tau + \ln C$, derived from the Lambert−Beer law and by assuming that bleaching exhibits first-order kinetics. C is a constant that ascribes to the thickness of the film, the concentration of the absorbing species, and their absorption cross-section. More details on the procedure of determining the time constant can be found in ref 26.

Composition analysis of the films was conducted by time-of-flight-energy elastic recoil detection analysis (ToF-E ERDA) at the Tandem Laboratory of Uppsala University, using 36 MeV I^{8+} ions as the primary beam. Scattered particles and recoils were detected by a set of two ToF foils and a segmented gas ionization chamber, located at 45° with respect to the incident beam.[27] ToF-E spectra were analyzed using Potku.[28] For structural characterization, X-ray diffraction (XRD) was conducted with a PANalytical Empyrean diffractometer with Cu−Kα radiation. The samples were measured in a grazing-incident geometry, keeping the incident angle at 1°. Pseudo-Voigt functions were used to identify the positions and widths of the Bragg peaks.

3. RESULTS AND DISCUSSION

Figure 2a presents the optical transmittance of YHO for the pristine film and after irradiation to fluences, Φ, of 330 keV Ne^+ irradiation ranging from 1×10^{12} to 1.5×10^{16} cm^{-2}. While fluences of less than 1×10^{14} cm^{-2} do not change optical transmittance significantly, a decrease by 48% is observed for $\Phi = 1 \times 10^{15}$ cm^{-2}. In comparison, the film irradiated to the same fluence but from the substrate side (the dashed line in Figure 2a) preserved its transmission, demonstrating that the optical transmittance of the glass substrate is not affected by ion irradiation. Thus, the observed changes in transmittance result from modifications of the YHO. It is well known that point defects created under ion irradiation can act as color centers and reduce optical

https://doi.org/10.1021/acs.jpcc.3c06010
J. Phys. Chem. C 2023, 127, 24676−24682

transmittance;[29,30] however, they typically feature pronounced absorption bands in contrast to what one observes for the samples irradiated by Ne. Further increase of ion fluence above 1×10^{15} cm^{-2} leads to a gradual decrease in transmittance with an increase by 30% for $\Phi > 1 \times 10^{16}$ cm^{-2}.

Similar to transmittance, the photochromic response remains almost unchanged at a level of 22% up to irradiation fluences $\leq 1 \times 10^{14}$ cm^{-2} (corresponding damage $\leq$0.03 dpa). After exposure to a fluence of 1×10^{15} cm^{-2}, the photochromic response decreased to 7.2% and almost vanished (<1.5%) for $\Phi > 5 \times 10^{15}$ cm^{-2}. At this irradiation level, on average, every single atom of the film was displaced from its original position at least once. Depending on the fluence, irradiation-induced changes in the optical properties may be reversible, as seen in Figure 2c, showing transmittance and photochromic response measured as a function of time elapsed since ion irradiation and normalized to the value of the pristine film. For $\Phi = 1 \times 10^{15}$ cm^{-2}, average transmittance recovered from 63 to 93% of its initial value after 1 month. A similar trend is observed for the photochromic response. On the other hand, the transmittance of the film exposed to $\Phi = 1 \times 10^{16}$ cm^{-2} increases only by 4% after 10 months, showing persistency of the introduced changes. Recovery of both transmittance and photochromic response at lower fluences may be an indication that the created defects (like Frenkel pairs) are prone to recombination even at room temperature. On the other hand, recombination at higher Φ is suppressed and can thus not be explained by a higher concentration of the same defects since in this case one would expect similar recovery rates. One plausible explanation of the reduced recovery rate is a segregation of defects forming more stable and complex defect structures.

To investigate potential changes in the crystalline structure of the films under irradiation, GIXRD was conducted. The results for fluences of 1×10^{13} and 1.5×10^{16} cm^{-2} are shown in Figure 2d. The five most pronounced peaks can be indexed as (111), (200), (220), (311), and (420) assuming a CaF_2-like structure. The dominance of the (200) peak is due to the strong texture of the films.[31] For an ion fluence $\geq 1 \times 10^{15}$ cm^{-2}, a shift of the Bragg peaks to larger angles (i.e., lattice contraction) is observed. This result might be associated with a H loss at higher fluences, as indicated from the chemical composition deduced from ToF-E ERDA (see Figure 2e). The full width at half-maximum (fwhm) of (111) peaks steadily decreases with increasing fluence, indicating that ion irradiation causes grain growth and improved crystallinity. Moreover, peak broadening in the XRD pattern can be associated with a residual stress which was reported for GdHO in ref 13. Thus, irradiation-induced stress relaxation might be an alternative explanation for the narrowing of the peaks. While peaks (200) and (311) for lower fluences are clearly skewed with a shoulder on the right side, the symmetry of those peaks, which can be assessed from the quality of the fit using the single peak function, is greatly improved for longer irradiation. For comparison, the coefficient of determination for $\Phi = 1 \times 10^{13}$ cm^{-2} is 0.993 against 0.999 for $\Phi = 1.5 \times 10^{16}$ cm^{-2}. Furthermore, additional peaks emerge for $\Phi \geq 1 \times 10^{16}$ cm^{-2} (especially visible at 35.7 and 60.2°) at the position of the peak shoulder. These peaks can be attributed to the orthorhombic YHO phase, which is a distorted CaF_2-like structure with ordered anions as reported in ref 32. Note, it is hard to unequivocally conclude whether this orthorhombic phase was present in the pristine sample or is formed under ion irradiation as small peaks might have been hidden in the shoulder of the (200) and (311) peaks. Nevertheless, it is, to the best of our knowledge, the first time when the orthorhombic YHO phase is reported in a thin film. Observed changes in the microstructure alongside the aforementioned defect complexes might be responsible for the irreversible modification of the optical properties at high fluences.

Figure 3a shows the effect of different irradiation conditions on the average optical transmittance; the data is presented as a function of dpa. For irradiations with a "high" S_e, damage below 0.1 dpa has little to no impact on the optical properties, while a larger number of atomic displacements rapidly reduced the transmittance down to 20% and less. Irradiations with Cl^{3+}, Ge^{3+}, and I^{5+} result in very similar reductions of transmittance. The result is expected as projectiles under these conditions having similar S_e, while the representation using dpa and not fluence eliminates the effect of differences in the S_n. However, irradiations with projectiles with a "low" S_e exhibit very different behavior. First, the damage threshold at which changes in optical transmittance start occurring depends on the S_n being 0.1 dpa for N^+ and ~0.65 dpa for Si^+. Second, the transmittance decrease rate (i.e., the slope of the trend) is also

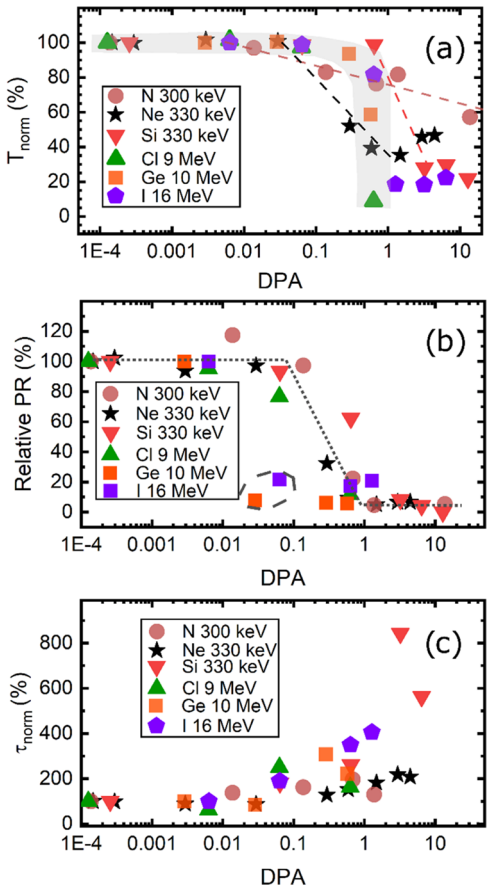

Figure 3. (a) Normalized average optical transmittance as a function of dpa for different irradiation conditions. Dashed lines are a guide to the eye and represent different exponential dependencies of T_{norm} on dpa. The gray area highlights the data points for irradiations with a "high" S_e. (b) Relative photochromic response and (c) bleaching time constant as functions of dpa for different irradiation conditions. The dotted line in panel (b) is a guide to the eye only (see the text). The dashed encircled area indicates a synergistic effect for energetic heavy ions with a high electronic and nuclear stopping power.

https://doi.org/10.1021/acs.jpcc.3c06010
J. Phys. Chem. C 2023, 127, 24676−24682

dependent on irradiation conditions becoming more steep for a higher S_n. For Si^+ and I^{5+}, one can see a change of the slope and/or a slight increase of transmittance when the damage is above 1 dpa. Similar to Ne^+ irradiation, this effect can be attributed to the phase transition and/or segregation of defects.

The normalized photochromic response as a function of dpa is depicted in Figure 3b. The dotted line is a guide to the eye showing a general trend. The photochromic effect starts to degrade for damages exceeding 0.05−0.1 dpa reaching values below 10% at ≥1 dpa. Results for Ge^{3+} and I^{5+} stand out from the general trend as a significant degradation of photochromic properties is observed already at 0.03 and 0.06 dpa (the dashed line in Figure 3b). Both projectiles feature relatively high S_n and S_e values in comparison to other irradiations. The impact on photochromism is larger than expected from the sum of separate electronic and nuclear processes, indicating a synergistic effect. The effect is especially evident for Ge, which features the S_n comparable with the S_n for Si (26.2 vs 26.8 2 eV/10^{15} at/cm^2), while its S_e (625.4 eV/10^{15} at/cm^2) is close to the S_e of Cl (616.3 eV/10^{15} at/cm^2). It has been demonstrated for several perovskite materials ($SrTiO_3$,[33] $KTaO_3$[34] $LiTaO_3$[35]) and MgO[36] that the presence of pre-existing defects (created by ion irradiation) can sensitize a material to electronic energy loss, resulting in enhanced damage due to defect-induced changes in the electronic and atomic thermal conductivity and increased electron−phonon coupling. Applying similar reasoning to the Ge and I irradiations presented here, one may suppose that irradiation at lower fluences creates defect structures that facilitate increased damage at higher fluences due to electronic loss. Additionally, one has to consider direct coupling between nuclear and electronic energy dissipation. When the energy is transferred to the electronic system of the material, processes like electron excitation and ionization taking place in the proximity of the ion track change the local electron distribution and rupture or modify the nature of bonds affecting atomic mobility by, for example, reducing displacement and binding energies. Thus, the damage calculated using SRIM may be underestimated when electronic energy loss is high, which might explain the degradation of photochromic response at lower damage levels for Ge^{3+} and I^{5+}.

The relaxation process is sensitive to ion irradiation (Figure 3c) as well. The bleaching time constant τ starts increasing noticeably at 0.06 dpa; a similar damage threshold was observed for the degradation of the photochromic response. The slowdown of the bleaching with increasing dpa is found for all irradiation conditions. While data points are quite scattered, they suggest that irradiations with lower S_n (Ne, N, and Cl) have a smaller effect on the bleaching speed than Si, Ge, and I with a high S_n. Supposing that the local diffusion of anions determines the bleaching process, the increase of anion vacancies under ion irradiation should promote a diffusion via hopping between interstitial sites and thereby increase the bleaching rate. On the other hand, XRD data revealed an increased grain size for higher fluences, which curbs a diffusion through grain boundaries. An increased τ might be an indication that an intergrain diffusion or a diffusion between two phases, as proposed in ref 13, is crucial for bleaching.

Figure 4 demonstrates the relation between the photochromic response and the optical transmittance of the samples after ion irradiation. The irradiation first affects the photochromic effect before transmission is affected, as reduced transmission is only observable for a weak residual photochromic effect. This result indicates that the system first transitions into a nonphotochromic state and only then starts accumulating defects that reduce optical transmittance, which are different in nature than the absorption sites in the photodarkened state.

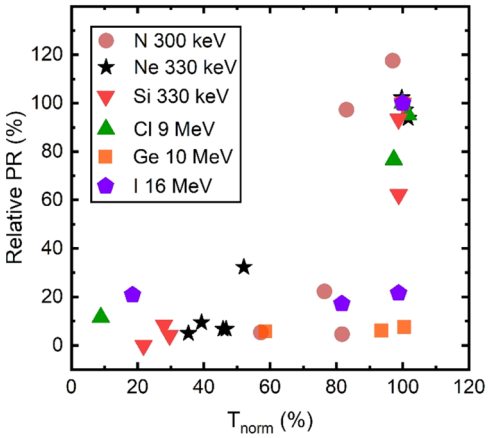

Figure 4. Correlation between the photochromic response and transmittance for ion-irradiated YHO samples. Both axes are normalized with respect to values for pristine samples.

While most of the proposed models explain the photochromic reaction in REHO as a result of the rearrangement of the local structure and short-distance migration of anions, in the current study we demonstrate that the defects introduced by irradiation with keV and MeV ions decrease both the photochromic response and the bleaching rate. Assuming that anion vacancies facilitate H or O migration, one could expect the opposite effect from ion irradiation. On the other hand, ion bombardment creates Y vacancies and possibly modifies the microstructure as well as induces phase transitions, all of which may affect the photochromic properties. To properly verify diffusion models, one would need to study the photochromic effect in the material with H or O deficiency (i.e., with abundant anion vacancies). Chaykina et al. proposed the aliovalent doping of YHO thin films.[16] While this approach indeed decreased H concentration, keeping the level of O unaffected, the number of Y atoms was found to be reduced. In ref 9, we have shown H loss and oxidation when YHO films are exposed to slightly elevated temperatures; therefore, annealing in an O-free environment can be an alternative way to introduce H vacancies without affecting other species.

4. SUMMARY AND CONCLUSIONS

Photochromic YHO thin films of 300 nm were irradiated with projectiles with an S_e of ≈70 eV/(10^{15} at/cm^2) (300 keV N^+, 330 keV Ne^+, and 330 keV Si^+) and of ≈620 eV/(10^{15} at/cm^2) (9 MeV Cl^{3+}, 10 MeV Ge^{3+}, and 16 MeV I^{5+}) to different fluences. Irradiation with Ne^+ resulted in a decrease in transmittance and photochromic response for $\Phi \geq 1 \times 10^{15}$ cm^{-2} and films showing almost no photochromism for $\Phi > 5 \times 10^{15}$ cm^{-2}. Introduced changes are reversible for $\Phi = 1 \times 10^{15}$ cm^{-2} probably due to the recombination of defects. Films irradiated to higher fluences show irreversible changes in optical properties and the microstructure and formation of defect complexes. Irradiation with a "high" S_e leads to a rapid reduction of transmittance for damages above 0.1 dpa, while for a "low" S_e, the decrease is gradual and starts at different dpa for different projectiles. Irradiations with considerably high S_n

https://doi.org/10.1021/acs.jpcc.3c06010
J. Phys. Chem. C 2023, 127, 24676−24682

and S_e, i.e., Ge^{3+} and I^{5+}, almost eliminate the photochromic effect at damages below 0.1 dpa, while the lack of photochromism is found only after reaching 1 dpa for other irradiations, indicating a synergistic effect. The bleaching process was found to be slower after irradiation. This observation together with the increase of grain size may indicate that diffusion through grain boundaries is involved in photochromism, in line with a dual-phase notion. The data show that irradiation to lower fluences can decrease photochromic properties without a significant effect on transmittance.

AUTHOR INFORMATION

Corresponding Author

D. Moldarev − *Department of Physics and Astronomy, Ångström Laboratory, Uppsala University, SE-751 20 Uppsala, Sweden;* orcid.org/0000-0003-3100-7144; Email: Dmitry.Moldarev@physics.uu.se

Authors

M. Wolff − *Department of Physics and Astronomy, Ångström Laboratory, Uppsala University, SE-751 20 Uppsala, Sweden;* orcid.org/0000-0002-7517-8204

D. Primetzhofer − *Department of Physics and Astronomy, Ångström Laboratory, Uppsala University, SE-751 20 Uppsala, Sweden;* orcid.org/0000-0002-5815-3742

Complete contact information is available at: https://pubs.acs.org/10.1021/acs.jpcc.3c06010

Notes

The authors declare no competing financial interest.

ACKNOWLEDGMENTS

The authors acknowledge financial support of the project by the Olle Engkvist Foundation under Grant Number 207−0423. Infrastructure support by VR-RFI [Grant #2019−00191]; supporting accelerator operation is gratefully acknowledged.

REFERENCES

(1) Nunes, D.; Pimentel, A.; Santos, L.; Barquinha, P.; Pereira, L.; Fortunato, E.; Martins, R.; Nunes, D.; Pimentel, A.; Santos, L.; et al. Chromogenic Applications. *Met. Oxide Nanostruct.* **2019**, 103−147, DOI: 10.1016/B978-0-12-811512-1.00004-7.

(2) Den Broeder, F. J. A.; Van Der Molen, S. J.; Kremers, M.; Huiberts, J. N.; Nagengast, D. G.; Van Gogh, A. T. M.; Huisman, W. H.; Koeman, N. J.; Dam, B.; Rector, J. H.; et al. Visualization of Hydrogen Migration in Solids Using Switchable Mirrors. *Nature* **1998**, *394* (6694), 656−658.

(3) Mongstad, T.; Platzer-Björkman, C.; Maehlen, J. P.; Mooij, L. P. A.; Pivak, Y.; Dam, B.; Marstein, E. S.; Hauback, B. C.; Karazhanov, S. Z. A New Thin Film Photochromic Material: Oxygen-Containing Yttrium Hydride. *Sol. Energy Mater. Sol. Cells* **2011**, *95* (12), 3596−3599.

(4) Nafezarefi, F.; Schreuders, H.; Dam, B.; Cornelius, S. Photochromism of Rare-Earth Metal-Oxy-Hydrides. *Appl. Phys. Lett.* **2017**, *111* (10), No. 103903.

(5) Adalsteinsson, S. M.; Moro, M. V.; Moldarev, D.; Droulias, S.; Wolff, M.; Primetzhofer, D. Correlating Chemical Composition and Optical Properties of Photochromic Rare-Earth Oxyhydrides Using Ion Beam Analysis. *Nucl. Instrum. Methods Phys. Res., Sect. B* **2020**, *485*, 36−40, DOI: 10.1016/j.nimb.2020.09.016.

(6) Moro, M. V.; Adalsteinsson, S. M.; Tran, T. T.; Moldarev, D.; Samanta, A.; Wolff, M.; Primetzhofer, D. Photochromic Response of Encapsulated Oxygen-Containing Yttrium Hydride Thin Films. *Phys. Status Solidi RRL* **2021**, *15* (6), No. 2000608, DOI: 10.1002/pssr.202000608.

(7) Strugovshchikov, E.; Pishtshev, A.; Karazhanov, S. Theoretical Design of Effective Multilayer Optical Coatings Using Oxyhydride Thin Films. *Phys. Status Solidi (b)* **2021**, *258* (10), No. 2100179.

(8) Kantre, K.; Moro, M. V.; Moldarev, D.; Wolff, M.; Primetzhofer, D. Synthesis and In-Situ Characterization of Photochromic Yttrium Oxyhydride Grown by Reactive e-Beam Evaporation. *Scr. Mater.* **2020**, *186*, 352−356.

(9) Moldarev, D.; Moro, M. V.; You, C. C.; Baba, E. M.; Karazhanov, S. Z.; Wolff, M.; Primetzhofer, D. Yttrium Oxyhydrides for Photochromic Applications: Correlating Composition and Optical Response. *Phys. Rev. Mater.* **2018**, *2* (11), No. 115203.

(10) Komatsu, Y.; Shimizu, R.; Sato, R.; Wilde, M.; Nishio, K.; Katase, T.; Matsumura, D.; Saitoh, H.; Miyauchi, M.; Adelman, J. R.; et al. Repeatable Photoinduced Insulator-to-Metal Transition in Yttrium Oxyhydride Epitaxial Thin Films. *Chem. Mater.* **2022**, *34* (8), 3616−3623.

(11) Kazi, S.; Moldarev, D.; Moro, M. V.; Primetzhofer, D.; Wolff, M. Correlating Photoconductivity and Optical Properties in Oxygen-Containing Yttrium Hydride Thin Films. *Phys. Status Solidi RRL* **2023**, *17* (5), No. 2200435, DOI: 10.1002/pssr.202200435.

(12) Moldarev, D.; Wolff, M.; Baba, E. M.; Moro, M. V.; You, C. C.; Primetzhofer, D.; Karazhanov, S. Z. Photochromic Properties of Yttrium Oxyhydride Thin Films: Surface versus Bulk Effect. *Materialia* **2020**, *11*, No. 100706.

(13) Hans, M.; Tran, T. T.; Adalsteinsson, S. M.; Moldarev, D.; Moro, M. V.; Wolff, M.; Primetzhofer, D. Photochromic Mechanism and Dual-Phase Formation in Oxygen-Containing Rare-Earth Hydride Thin Films. *Adv. Opt. Mater.* **2020**, *8* (19), No. 2000822.

(14) Ohmura, A.; Machida, A.; Watanuki, T.; Aoki, K.; Nakano, S.; Takemura, K. Photochromism in Yttrium Hydride. *Appl. Phys. Lett.* **2007**, *91* (15), No. 151904.

(15) Wu, Z.; de Krom, T.; Colombi, G.; Chaykina, D.; van Hattem, G.; Schut, H.; Dickmann, M.; Egger, W.; Hugenschmidt, C.; Brück, E.; et al. Formation of Vacancies and Metallic-like Domains in Photochromic Rare-Earth Oxyhydride Thin Films Studied by in-Situ Illumination Positron Annihilation Spectroscopy. *Phys. Rev. Mater.* **2022**, *6* (6), No. 65201, DOI: 10.1103/PhysRevMaterials.6.065201.

(16) Chaykina, D.; Usman, I.; Colombi, G.; Schreuders, H.; Tyburska-Pueschel, B.; Wu, Z.; Eijt, S. W. H.; Bannenberg, L. J.; de Wijs, G. A.; Dam, B. Aliovalent Calcium Doping of Yttrium Oxyhydride Thin Films and Implications for Photochromism. *J. Phys. Chem. C* **2022**, *126* (34), 14742−14749.

(17) Chaykina, D.; Nafezarefi, F.; Colombi, G.; Cornelius, S.; Bannenberg, L. J.; Schreuders, H.; Dam, B. Influence of Crystal Structure, Encapsulation, and Annealing on Photochromism in Nd Oxyhydride Thin Films. *J. Phys. Chem. C* **2022**, *126* (4), 2276−2284.

(18) Privitera, S. M. S.; Rimini, E. Ion Beam Irradiation of Phase Change Materials: A Route to Material Properties Investigation and Engineering. *Mater. Sci. Semicond. Process.* **2021**, *135*, No. 106087.

(19) Rahman, M. M.; Chen, W.-Y.; Mu, L.; Xu, Z.; Xiao, Z.; Li, M.; Bai, X.-M.; Lin, F. Defect and Structural Evolution under High-Energy Ion Irradiation Informs Battery Materials Design for Extreme Environments. *Nat. Commun.* **2020**, *11* (1), No. 4548.

(20) Zhang, Y.; Weber, W. J. Ion Irradiation and Modification: The Role of Coupled Electronic and Nuclear Energy Dissipation and Subsequent Nonequilibrium Processes in Materials. *Appl. Phys. Rev.* **2020**, *7* (4), No. 041307, DOI: 10.1063/5.0027462.

(21) Tran, T. T.; Bruce, H.; Pham, N. H.; Primetzhofer, D. A Contactless Single-Step Process for Simultaneous Nanoscale Patterning and Cleaning of Large-Area Graphene. *2D Mater.* **2023**, *10* (2), No. 025017.

(22) Sun, C.; Wang, P.; Wang, H.; Xu, C.; Zhu, J.; Liang, Y.; Su, Y.; Jiang, Y.; Wu, W.; Fu, E.; Zou, G. Defect Engineering of Molybdenum Disulfide through Ion Irradiation to Boost Hydrogen Evolution Reaction Performance. *Nano Res.* **2019**, *12* (7), 1613−1618.

(23) Ström, P.; Primetzhofer, D. Ion Beam Tools for Nondestructive In-Situ and in-Operando Composition Analysis and Modification of

Materials at the Tandem Laboratory in Uppsala. *J. Instrum.* **2022**, *17* (04), No. P04011.
(24) Ziegler, J. F.; Ziegler, M. D.; Biersack, J. P. SRIM − The Stopping and Range of Ions in Matter (2010). *Nucl. Instrum. Methods Phys. Res., Sect. B* **2010**, *268* (11−12), 1818−1823.
(25) Moldarev, D.; Komander, K.; Holeňák, R.; Wolff, M.; Primetzhofer, D. A New Setup for Optical Measurements under Controlled Environment. *Rev. Sci. Instrum.* **2023**, *94* (3), No. 35104, DOI: 10.1063/5.0142068.
(26) Nafezarefi, F.; Cornelius, S.; Nijskens, J.; Schreuders, H.; Dam, B. Effect of the Addition of Zirconium on the Photochromic Properties of Yttrium Oxy-Hydride. *Sol. Energy Mater. Sol. Cells* **2019**, *200*, No. 109923, DOI: 10.1016/j.solmat.2019.109923.
(27) Ström, P.; Petersson, P.; Rubel, M.; Possnert, G. A Combined Segmented Anode Gas Ionization Chamber and Time-of-Flight Detector for Heavy Ion Elastic Recoil Detection Analysis. *Rev. Sci. Instrum.* **2016**, *87* (10), No. 103303, DOI: 10.1063/1.4963709.
(28) Arstila, K.; Julin, J.; Laitinen, M. I.; Aalto, J.; Konu, T.; Kärkkäinen, S.; Rahkonen, S.; Raunio, M.; Itkonen, J.; Santanen, J.-P.; et al. Potku − New Analysis Software for Heavy Ion Elastic Recoil Detection Analysis. *Nucl. Instrum. Methods Phys. Res., Sect. B* **2014**, *331*, 34−41.
(29) Song, Y.; Zhang, C.; Yang, Y.; Gou, J.; Zhang, L.; He, D. Color Center Creation in SiO2 under Irradiation with Swift Heavy Ions: Dependence on Energy Loss and Fluence. *Opt. Mater.* **2013**, *35* (5), 1057−1061.
(30) Schwartz, K.; Sorokin, M. V.; Lushchik, A.; Lushchik, C.; Vasil′chenko, E.; Papaleo, R. M.; de Souza, D.; Volkov, A. E.; Voss, K.-O.; Neumann, R.; Trautmann, C. Color Center Creation in LiF Crystals Irradiated with 5- and 10-MeV Au Ions. *Nucl. Instrum. Methods Phys. Res., Sect. B* **2008**, *266* (12), 2736−2740.
(31) Maehlen, J. P.; Mongstad, T. T.; You, C. C.; Karazhanov, S. Lattice Contraction in Photochromic Yttrium Hydride. *J. Alloys Compd.* **2013**, *580*, S119−S121.
(32) Zapp, N.; Auer, H.; Kohlmann, H. YHO, an Air-Stable Ionic Hydride. *Inorg. Chem.* **2019**, *58* (21), 14635−14641.
(33) Weber, W. J.; Zarkadoula, E.; Pakarinen, O. H.; Sachan, R.; Chisholm, M. F.; Liu, P.; Xue, H.; Jin, K.; Zhang, Y. Synergy of Elastic and Inelastic Energy Loss on Ion Track Formation in SrTiO3. *Sci. Rep.* **2015**, *5* (1), No. 7726.
(34) Velişa, G.; Wendler, E.; Wang, L.-L.; Zhang, Y.; Weber, W. J. Ion Mass Dependence of Irradiation-Induced Damage Accumulation in KTaO3. *J. Mater. Sci.* **2019**, *54* (1), 149−158.
(35) Han, X.; Liu, Y.; Crespillo, M. L.; Zarkadoula, E.; Huang, Q.; Wang, X.; Liu, P. Latent Tracks in Ion-Irradiated LiTaO3 Crystals: Damage Morphology Characterization and Thermal Spike Analysis. *Crystals* **2020**, *10* (10), No. 877, DOI: 10.3390/cryst10100877.
(36) Thomé, L.; Debelle, A.; Garrido, F.; Trocellier, P.; Serruys, Y.; Velisa, G.; Miro, S. Combined Effects of Nuclear and Electronic Energy Losses in Solids Irradiated with a Dual-Ion Beam. *Appl. Phys. Lett.* **2013**, *102* (14), No. 141906, DOI: 10.1063/1.4801518.

https://doi.org/10.1021/acs.jpcc.3c06010
J. Phys. Chem. C 2023, 127, 24676−24682